Environmental Science
Atmospheres

Accepted Manuscript

This article can be cited before page numbers have been issued, to do this please use: Z. Cheng, D. Hu, M. Flynn, E. Nemitz, B. Langford, W. Drysdale, C. Helfter, S. Cliff, D. Liu, R. Joshi, J. Cash, J. D. Lee, H. Coe and J. Allan, *Environ. Sci.: Atmos.*, 2025, DOI: 10.1039/D5EA00039D.

ROYAL SOCIETY OF CHEMISTRY

rsc.li/esatmospheres

View Article Online
DOI: 10.1039/D5EA00039D

Black Carbon (BC) has significant health effect, but no direct observation of urban BC emissions has been made in Europe. Quantifying BC emissions and understanding their sources can help make attempts to control BC concentrations and thereby reduce associated health risks. This study presents the first eddy covariance measurement across Europe, highlighting the construction contribution to BC emissions in central London, while inventory overestimates this source by a factor of five. Inventory uncertainties will propagate to models and affect policy decisions. The results also enhance the confidence of BC emissions using eddy covariance by comparing with previous results in Beijing and Delhi. Thus, this study also supports the improvement of air quality management and policy development across different regions.

Quantifying Black Carbon emissions from Traffic and Construction in central London using Eddy Covariance

Zixuan Cheng[1], Dawei Hu[1], Michael Flynn[1], Eiko Nemitz[2], Ben Langford[2], Will Drysdale[3,4], Carole Helfter[2], Samuel Cliff[3,5], Dantong Liu[6], Rutambhara Joshi[7], James Cash[2], James Lee[3,4], Hugh Coe[1,8] and James Allan[1,8]

[1] Department of Earth and Environmental Sciences, The University of Manchester, Manchester, M13 9PL, UK
[2] UK Centre for Ecology and Hydrology, Bush Estate, Penicuik, EH26 0QB, UK
[3] Wolfson Atmospheric Chemistry Laboratories, Department of Chemistry, University of York, York, YO10 5DD, UK
[4] National Centre for Atmospheric Science, University of York, York, YO10 5DD, UK

[5] now at: Department of Civil and Environmental Engineering, University of California Berkeley, Berkeley, CA 94720, United States.
[6] Department of Atmospheric Sciences, School of Earth Sciences, Zhejiang University, Hangzhou, Zhejiang, 310027, China
[7] UK Centre for Ecology and Hydrology, Maclean Building, Wallingford, OX10 8BB, UK

[8] National Centre for Atmospheric Science, The University of Manchester, Oxford Road, Manchester, M13 9PL, UK

Correspondence to: James Allan (James.allan@manchester.ac.uk)

Abstract.

Black carbon (BC) is a significant environmental health and climate forcing concern. Direct measurement of BC fluxes using eddy covariance can quantify emissions and identify sources. Previous studies have examined urban BC emissions in highly polluted countries such as China and India, but to date no equivalent research has been done in the UK and Europe. Here, we present black carbon flux data from Single Particle Soot Photometer (SP2) deployed in an eddy covariance system at the BT (formerly British Telecommunications) Tower in central London. Mean BC mass (number) fluxes with size range 60nm to 600nm were 6.83 ng m^{-2} s^{-1} (443 cm^{-2} s^{-1}) in summer and 13.3 ng m^{-2} s^{-1} (687 cm^{-2} s^{-1}) in winter, indicating relatively low BC emission when compare to Delhi, which is likely due to the introduction of the Ultra Low Emission Zone (ULEZ) and road diesel vehicles to be Euro 6 or higher. However, flux footprint analysis identified strong point sources near construction sites during winter and summer observations, which implies Non-Road Mobile Machinery (NRMM) emissions can dominate over traffic BC emissions. This implies tightened NRMM regulations can help future air quality in London. Observations indicate that the UK's National Atmospheric Emissions Inventory (NAEI) overestimate BC emissions by a factor of 5, although large uncertainties are expected for the sector Combustion in manufacturing industry. The estimate of traffic emissions is more accurate.

1 Introduction

Fine particulate matter ($PM_{2.5}$) is a large environmental health concern and results in 4.2 million premature deaths per year [1]. Black carbon (BC) is a carbonaceous material formed by incomplete combustion [2] that comprises an important fraction of $PM_{2.5}$. Epidemiological evidence suggests that BC can cause respiratory diseases, cardiovascular diseases, and adverse effects on nervous system [3-5]. In densely populated urban areas, people are more likely to be exposed to higher concentrations of BC [6]. Furthermore, BC is second only to greenhouse gases (GHGs) in radiative forcing and warming of the atmosphere via the direct absorption of solar radiation [2]. However, unlike GHGs, which mostly have an atmospheric lifetime of tens to hundreds of years, the BC lifetime is usually a few days to a week. Therefore, the mitigation of emissions will reap climate benefits on a much faster timescale [7].

London is the capital city of the U.K. with a population of 8.8 million and is facing a significant health burden from air pollution that includes the inhalation of BC. To reduce this health burden and meet WHO guidelines for the annual mean of $PM_{2.5} \leq 5$ $\mu g\ m^{-3}$, the world's first ultra-low emission zone (ULEZ) was introduced by Greater London Authority (GLA) in April 2019 and then expanded to cover the whole central London encompassing 4 million people in October 2021. Drivers of motorcycles, petrol vehicles and diesel cars are charged to drive in the ULEZ if they failed to meet Euro 3, Euro 4 and Euro 6 exhaust emissions standards, respectively [8]. Of particular note, the requirement for Euro 6 diesel heavy-duty vehicles could have a major impact on $PM_{2.5}$ emissions (g/km) with a regulatory limit more than 20 times stricter than that of Euro 5. Additionally, the BC fraction within $PM_{2.5}$ is reduced from 75% to 15% [9]. Recent studies suggest that one year after the ULEZ was implemented, nitrogen oxides (NOx), carbon dioxides (CO_2) and $PM_{2.5}$ emissions within the zone have reduced by 19%, 4% and 7%, respectively [10].

Atmospheric models are typically used by local government to estimate and predict the effectiveness of policies. Atmospheric models often use atmospheric inventories as data input [11]. The National Atmospheric Emissions Inventory (NAEI) is a widely used inventory in the U.K. as the official UK estimate of sources and trends in emissions of air pollutants and greenhouse gas (GHG) [12]. However, atmospheric inventories contain uncertainties caused by (1) the complexity and variability (e.g., temporal and spatial distribution of activities) of emission sources when collecting data, (2) the estimate methodology uncertainties, such as quality control of mapping approach [13, 14] and (3) the complexity of chemistry and meteorological process such as NO_x [11]. These uncertainties will propagate to atmospheric models and cause models prediction errors [15]. Therefore, inventory verification is important to ensure inventories correctly represent emissions by sectors. Direct observation of fluxes can provide evaluation of inventories by comparing the measured fluxes with inventory emission rates as they have the same units and physical meanings.

The eddy covariance (EC) method provides a direct flux measurement for a species of interest that is emitted from or deposited to the surface. In addition, spatial information on emissions sources can be obtained via flux footprint analysis (FFP). Although more typically used to measure GHG, sensible heat and latent heat exchange of vegetation, the use of EC has expanded to aerosols and variable surfaces including urban environments [16, 17]. For example, EC to be applied on a grassland to measure

BC deposition [18] and within urban areas to quantify BC emissions in Beijing and Delhi[17, 19]. At the time of writing, there have been no studies using EC to measure BC emissions within European urban areas.

In this paper, we quantify urban BC emissions in London with an EC system deployed on a 190-meter tower in central London during the summer and winter of 2021. Each season includes a 1-month-long intensive observation campaign. BC concentrations and characterization was measured by a Single Particle Soot Photometer (SP2; Droplet Measurement Technologies, Boulder, USA). Furthermore, FFP analysis was applied to quantify the contribution of BC emissions spatially and identify the highlighted sources. A comparison between Delhi, Beijing and London was also carried out to initially evaluate difference in BC emissions among cities.

2 Methodology

2.1 Measurement site location

Fluxes of BC were measured intensively in both summer and winter from BT tower (51∘31′17.4″ N, 0∘8′20.04″ W; 190 m) operated by BT GROUP PLC for telecommunications and urban atmospheric pollution observation in central London. The mean building height is 8.8 ± 3 m within 10 km from BT tower. Hyde Park and The Regent's Park are located 1.5 km southwest and 1 km northwest, respectively, of the tower. The surrounding surface is a high-density human activity area including busy roads, shopping centres and construction sites.

The EC system at the BT tower consists of a 3D ultrasonic anemometer (R3-50, Gill Instruments, Lymington, UK) operating at 20 Hz [20], deployed together with the SP2 sample line inlet as described below. The SP2 was deployed in an air-conditioned room located on 35th floor of the 44-storey tower, subsampling from a 45 m 1/2'' outside diameter, 3/8" inside diameter copper tube. The impact and uncertainty caused by the long tube will be discussed in Section 2.4.

2.2 BC measurements and calibrations

Refractory Black Carbon (rBC) is operationally defined as the BC measured by Laser-Induced Incandescence (LII). The concentrations and physical properties of rBC particles were quantified and characterised using a Single Particle Soot Photometer (SP2) based on LII technology [21, 22]. The sample flow containing the BC was interacted with an intra-cavity Nd:YAG Gaussian laser beam at 1064 nm pumped by diode laser inside the SP2 chamber. rBC absorbs laser light and emits incandescence light, while non-rBC materials only scatter the laser light. The emitted and scattered light from individual particles is detected as incandescence and scattering signals by the Avalanche Photodiode Detector (APD) in the optical head of the SP2. Every rBC containing particle, which can trigger incandescence and scattering channel, in the sample flow should be recorded under ideal conditions. However, due to the limitation of hard drive space, the sampling frequency was set to 1 in 3 particles in winter and 1 in 2 particles in summer in this study.

SP2 can measure ambient BC because 1064 nm light is mainly absorbed by BC in the atmosphere. In this study, quantitative rBC mass concentrations were calculated from the incandescence signal measured by SP2 based on calibrations with Aqueous Deflocculated Acheson Graphite (Aquadag), standard BC particle with known size and mass. A correction coefficient of 0.75 was applied to account for the difference in the light absorption of Aquadag compared with ambient BC [23, 24]. Number concentrations of rBC containing particles were determined directly from the statistics of the incandescence signal.

BC particles can be simulated by the core-shell model, which means a concentric sphere with a BC core and non-BC material around the core, also known as coatings [25]. The BC core diameter (Dc) is converted from rBC mass using BC atmosphere density (ρ = 1.8 g cm^{-3}). BC particle size including any coatings is derived from the scattering signal of the SP2. However, coatings of BC particles can vaporize because the laser heats particles, causing a collapse of the scattering signal. The collapse signal can be reconstructed using the scattering signal before vaporization, through what is called a Leading-Edge-Only (LEO) fit [21, 23]. The coating of BC is quantified using the Scattering Enhancement method [23, 26], the parameter of Scattering Enhancement method Esca is defined as Eq. (1):

$$\mathrm{Esca} = \frac{S_{\mathrm{measured,\ coated}}}{S_{\mathrm{calculated,uncoated}}}, \quad (1)$$

where $S_{\mathrm{measured,\ coated}}$ represents the scattering signal of BC particle with any coatings measured by the SP2 after LEO fitted and scattering channel calibration using polystyrene latex (PSLs; Thermo Fisher Scientific), and $S_{\mathrm{calculated,uncoated}}$ is the scattering signal of the corresponding BC core without any coatings, calculated using BC core refractive index at SP2 laser wavelength 1064 nm [26-28]. From this definition, for a given BC core, Esca = 1 means no coating, while a larger Esca implies a thicker coating enveloping BC core.

In this study, the Esca analysis was not applied in the summer campaign because the calibration could not be performed due to Covid restrictions. Aquadag calibrations were conducted in the lab after the summer campaign. Aquadag calibrations in winter were conducted at the Birmingham Air Quality Supersite (BAQS) after the BT tower campaign, during which a one-month SP2 measurement was undertaken using the same SP2 as in London. Therefore, a PSL calibration with the same SP2 was conducted upon returning to the lab after the winter campaign.

2.3 BC flux calculation

The BC flux (F_{BC}) was derived as the covariance between instantaneous fluctuations of BC concentrations (C'_{BC}) and vertical wind speed (w') [29]. The fluctuations were derived by Reynolds decomposition. For example, for BC concentrations fluctuations can be calculated as Eq. (2):

$$C'_{BC} = C_{BC} - \overline{C_{BC}}, \quad (2)$$

where C_{BC} is the BC concentration measured by SP2 at 5 Hz, and $\overline{C_{BC}}$ is the arithmetic mean of C_{BC} over the 30-minute average interval. Then BC flux can be calculated following Eq. (3):

$$F_{BC} = \overline{w'C'_{BC}}, \quad (3)$$

Here F_{BC} is the BC flux equal to the covariance of BC instantaneous fluctuation (C'_{BC}) and vertical wind speed instantaneous fluctuation (w') over 30 minutes. In the atmosphere, turbulent eddies provide the dominant vertical transport mechanism for most scalars (e.g. air pollutant concentrations). The 30 minutes average interval is sufficient to capture most eddies and whilst also avoid most non-stationarities during interval such as synoptic changes [29-31].

The entities w' and C'_{BC} are recorded with a time lag caused by the 45 m sample line separating the sonic anemometer and SP2, which needs to be removed prior to application of Eq. (3). This time lag was estimated by maximization of covariance method[16, 17]. Here, the time lag is calculated every 24 hours in 3 weeks at beginning, middle and end of each campaign. In this study, the median lag times were 9 s in summer and 7 s in winter.

F_{BC} calculations were performed using EddyPro (version 7.0.6, LI-COR lnc.), open-source software developed for calculating EC fluxes, especially for greenhouse gas (GHG) fluxes. Sonic anemometer data were resampled using trapezoidal average to the same time resolution (5 Hz) as C_{BC}.

2.4 Corrections and quality control

The EC method requires several assumptions to reduce flux uncertainties and to ensure that the measured flux is representative of the surface exchange [32, 33]. The sample inlet is deployed at the height 190 m, which is more than ten times higher than the urban canopy around (averaged 12 m). Furthermore, the measurement can represent the area of interest for the prevailing wind directions because of the height. EC assumes that wind speed and scalars are measured in the constant flux layer which turbulence properties are vertically uniform. However, the BT tower measurements height may extend above the constant flux layer which is defined as lowest 10% of the boundary layer [34]. In such case, the EC flux would underestimate the surface exchange due to vertical flux divergence (VFD) caused by storage, advection and boundary layer entrainment [35, 36]. VFD are the function of measurement heights, constant flux heights and entrainment heights (80% of boundary layer height). This implies that VFD uncertainty becomes noticeable when measurement heights reach entrainment heights. During both BT tower campaign, the boundary layer heights (BLH) were estimated from ECMWF Reanalysis global meteorology product (ERA5) and corrected using the factor described previously [36]. The BLH diurnal profile (Figure S6) shows mean scaled BLH around 500 m even in the evening, indicating that entrainments heights are much higher than measurement height. Applying VFD corrections leads to 22% (summer) and 15% (winter) increase of the averaged mass fluxes when using ERA5 BLH. If the scaled BLH is used, the increase is changed to 21% (summer) and 1% (winter). However, due to the uncertainties in the BLH data and scaling factor (Pearson correlation factor 0.59[36]), applying the VFD corrections may introduce additional low

frequency error to the total flux. Therefore, VFD corrections were not applied in this study. Nonetheless, we recommend that future studies at BT tower include direct BLH measurements, along with concentration profile between ground and the observation height. In addition, to ensure horizontal terrain and turbulent flux transformation, we applied 1) tilt corrections 2) stationarity test and 3) friction velocity test. The EC method also has significant uncertainties for low and high frequency [29]. Here, we applied spectral analysis to estimate the low and high frequency loss.

2.4.1 Tilt corrections

Tilt corrections allow correcting the measured wind speed to align with the average wind flow line to ensure the mean value of fluctuations is zero. Double rotation [37] is applied here to each 30-minute data segment to rotate the coordinates to align one wind component (u) with the mean wind flow and nullify the 30-minute means of the cross-wind (v) and vertical (w) wind components.

Equation (3) in Section 2.3 requires removal of the average of signals from fluctuations under ideal stationary conditions. However, ideal stationary, steady-state conditions are uncommon in the real atmosphere. Linear detrending of each 30 minutes intervals allows to remove long term (low frequency) trends from fluctuations, which has no contributions to total fluxes [38]. Here, we applied linear detrending to remove the low frequency trend which is specifically SP2 BC concentration variation within the 30-minute average interval.

2.4.2 Stationarity and friction velocity corrections

At night, the absence of solar heating impedes turbulence development. This low-turbulence boundary layer at night may induce non-stationary because advection flow dominates pollutant transport and enables accumulation (storage) of material released from the surface below the measurement. Suppressed vertical mixing increases the flux footprint resulting in measuring fluxes outside the area of interest. These advection processes present challenges to EC measurements, which quantify vertical transport between the surface and the atmosphere. For this reason, fluxes were flagged and filtered based on stationarity tests and friction velocity criteria.

To ensure that 30-minute average intervals meets the assumption of turbulence statistically invariant, we applied a stationarity test [39] in which the 30-minute flux interval was divided to six sub-intervals, and the fluxes of sub-intervals are calculated. The stationarity test compares the 30 minutes fluxes with the average of the sub-intervals' fluxes. If the difference exceeded 30%, the 30-minute interval flux was flagged and filtered out. After applying the stationarity test, 10.8% (mass), 11.6% (number) in summer and 12.7% (mass) 11.2% (number) in winter data points were removed, and the fluxes increased 7.50% (mass) and 9.00% (number) in summer and 9.90% (mass) 12.0% (number) in winter.

Friction velocity (u_*) serves as a metric for assessing the vertical transport efficiency of atmospheric turbulence and the pollutants. To ensure that the turbulence is fully developed, the flux intervals with $u_* < 0.2$ m/s were filtered [11, 30, 35, 36].

2.4.3 Negative fluxes

In EC measurements, positive fluxes represent net surface-to-atmosphere transport (emission), while negative fluxes indicate the opposite (deposition). To better address that, exchange velocity (V_{ex}) in winter was calculated by $V_{ex} = F_{BC}/\overline{C_{BC}}$ for each 30-minute interval as shown in Figure S1, positive V_{ex} indicates net emission while negative indicates net deposition. Emission and deposition can occur simultaneously over urban surface [16]. The deposition flux (F_{dep}) can be determined by:

$$F_{dep} = -C \times V_d \quad (4)$$

Where C is the concentration of interest scalar (BC) and V_d is the corresponding deposition velocity. V_d for BC was observed as 0.3 ± 0.2 mm s^{-1} over grassland [18], however, there is no information on BC V_d to urban surfaces. Particles V_d over urban surfaces can be estimated using sulfate (SO_4^{2-}), which is a function of u_* [16], to be 0 to 3.5 mm s^{-1} for u_* 0 to 1 m s^{-1} which is larger than grassland. This indicates the morphology of surface elements would affect the V_d [16]. So V_d is consist in a 30-mintues interval, while concentration variability can influence the deposition fluxes, potentially exceeding emission and resulting in negative fluxes.

During winter measurements, three periods of sustained negative fluxes were observed (2021/12/18 0:30 - 2021/12/18 9:00; 2021/12/24 18:00 – 2021/12/25 8:00; 2021/12/25 18:00 - 2021/12/26 7:00) after applying the corrections as discussed above. These periods accounted for 4% of the total flux. We noted that there is no distinct spike in BC concentration (Figure S4) during these periods, suggesting that the deposition was low. The precipitation washout of BC could have reduced BC concentration, leading to suppressed deposition flux. Neither the double rotation application nor flow distortion could be identified as reasons for the negative flux (Figure S1, S2). Large downward momentum fluxes were observed during these periods (Figure S1), suggesting that the reservoir of BC above the measurement height may be responsible for the negative fluxes in this study. To address this, we applied a 24-hour NOAA backward trajectory analysis model to estimate the sources of the BC reservoir (Figure S3). Air movements above the measurement height during the negative flux periods are shown to transport from the European continent, possibly due to additional BC emissions related to holiday activities (Christmas). Thus, these negatives fluxes were removed from total fluxes as deposition period.

2.4.4 Spectra analysis

Mixing in inlet lines results in high-frequency losses in closed-path EC system, which were evaluated using spectra analysis. This loss greatly increases under laminar flow conditions which therefore need to be avoided [29]. An effective way is to run at high flow rates to avoid laminar flow. Turbulent flow can be quantified via the Reynolds number (Re) and the high frequency losses can be corrected according to Re as described previously [36]. Co-spectral density, which indicates the covariance of vertical wind speed (w) and scalar (BC number and mass concentration) in frequency domain, are calculated using Fast Fourier Transport (FFT). The frequency is normalised by multiplying measurement hight ($z-z_d$; $z_d = 0.67 \times$ canopy height) and then dividing by wind speed ($f(z-z_d)/u$), which can coincident the frequency into inertial subrange. While co-spectra densities are normalised by multiplying natural frequency and dividing by the covariance flux to bring both co-spectra to approximately the

same level. Normalised co-spectra collapse into universal curves allowing to evaluate the contribution of each frequency band to the total flux. Negative normalised co-spectra mean momentum (w) and scalar (BC) are transported in different directions, indicates negative contribution to total flux. Since sensible heat fluxes (HF) is measured with a sonic anemometer which has a higher time resolution and measures at the top of the tower without any tubes, HF spectra often use as reference spectra [17, 18]. Normalised F_{BC} and HF cospectra were compared for both campaigns as shown in Figure 1. HF co-spectra satisfied the energy cascade ideal $f^{-4/3}$ relationship [40] in the inertial subrange which improves the confidence in using HF cospectra as reference cospectra. In the two seasons, BC exhibits a shape similar to the reference spectrum (HF) across nearly all frequencies, except for losses in the high-frequency range (>10 Hz). To address this high-frequency loss, we applied the Ogives analysis [41, 42], which calculates cumulative spectra starting from high frequencies, thus facilitating a more precise evaluation of the high-frequency losses. Difference between F_{BC} Ogive (Figure 2, black) and HF Ogive (Figure 2, red) are less than 10%. Winter Ogive was scaled using factor of 0.96 resulting to 6.8% flux losses, while summer Ogive was scaled using factor of 0.90 resulting to 9.9% flux losses as shown in Figure S9. This reflects the large eddy size at the BT Tower height and is consistent with other BT Tower based studies [30, 36]. In summary, high-frequency correction was not applied here.

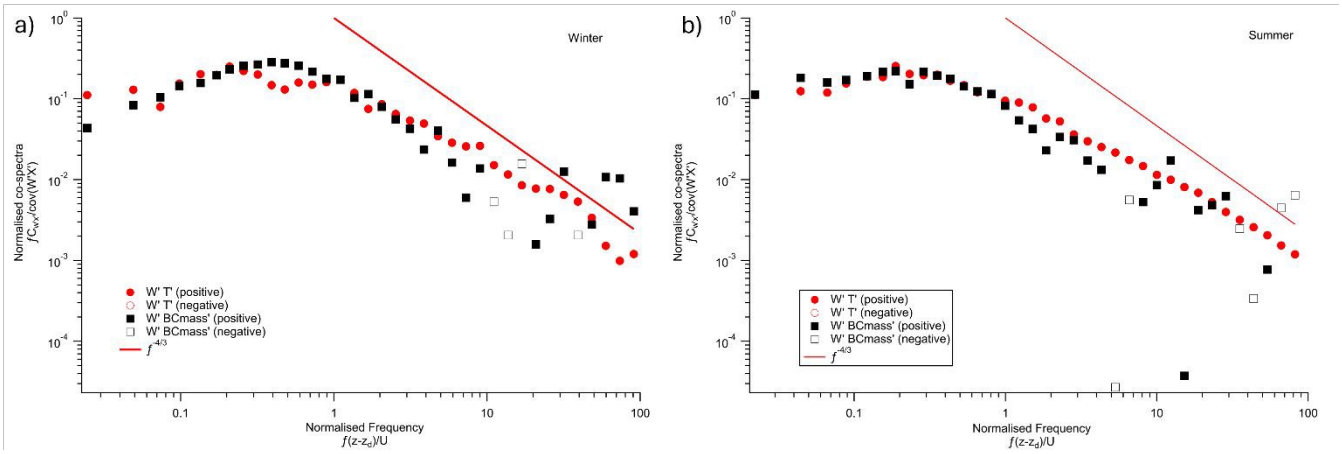

Figure 1: Co-spectra analysis in winter (194 cases, a) and summer (201 cases, b) which are binned into 40 even space bins. BC flux < 0 ng^{-2} s^{-1} and u_*< 0.2 m s^{-1} co-spectra are removed. Empty marks indicate negative contribution to total flux and are negated when plotting.

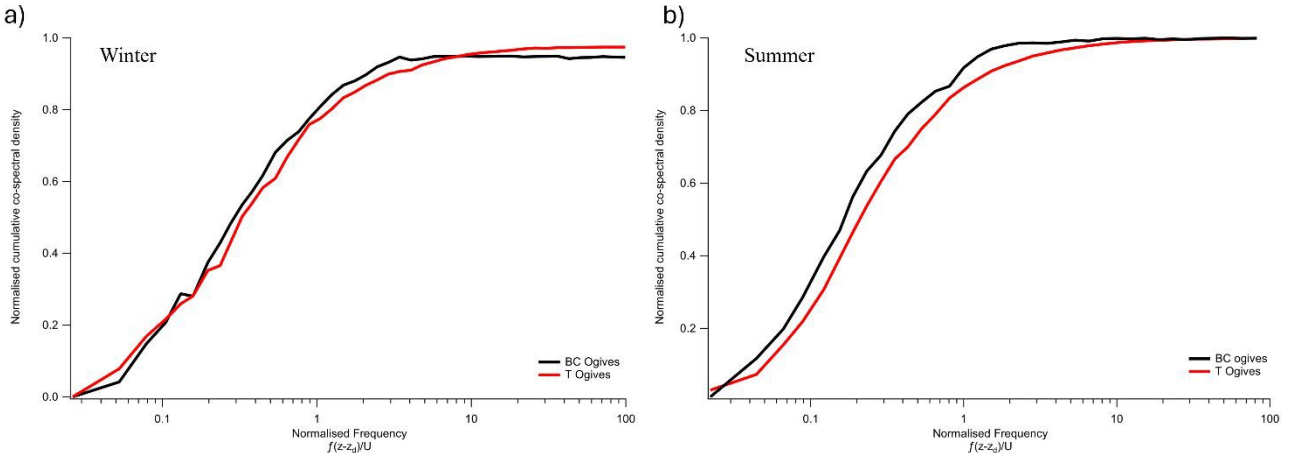

Figure 2: Normalised cumulative co-spectra (Ogives) of BC flux (black) and HF (red) in winter (a) and summer (b).

2.5 Footprint modelling

The flux footprint (FFP) refers to the area in the prevailing upwind direction that contributes to the measured fluxes. Here, a parameterized version of the Lagrangian backward model based on EddyPro was applied to determine to the distance to the footprint maximum of each 30-minute flux measurement, which represents the location of maximum contribution to the flux [43]. This footprint maximum is then mapped onto a geographical map using R-based OpenAir package [44] following an approach as described previously [36]. In short, the approach uses the maximum distance of the footprint to replace wind speed in producing a wind rose plot and maps the plot to geographical coordinates (latitude and longitude).

2.6 NOx, CO measurements and activities data

Long-term NO and NO_2 measurements using a dual-channel chemiluminescence analyser (Air Quality Design Inc., Boulder Colorado, USA; 5 Hz), began in September 2020 at BT tower [35, 36], whilst long-term CO measurements at the tower were made as part of UKCEH's National Capability programme, historically with an Aerolaser fast CO monitor (Model AL5002) at 10 Hz [30] and during these campaigns with a dual quantum cascade laser direct absorption spectrometer (Aerodyne Research Inc., USA). NOx and CO fluxes were all calculated using the EC method and shared the same ultrasonic anemometer and inlet described in Section 2.1.

Traffic data were from Transport for London (TfL) via a freedom-of-information request during the measurement campaigns [35]. NRMM type, power rating EU emission standard stage, approval number and exemption covering footprint area during both campaigns were also provided by Greater London Authority (GLA) via a freedom-of-information request [45]. However, the specific site name was not provided due to data protection regulations.

3 Results and discussions

3.1 BC mixing state

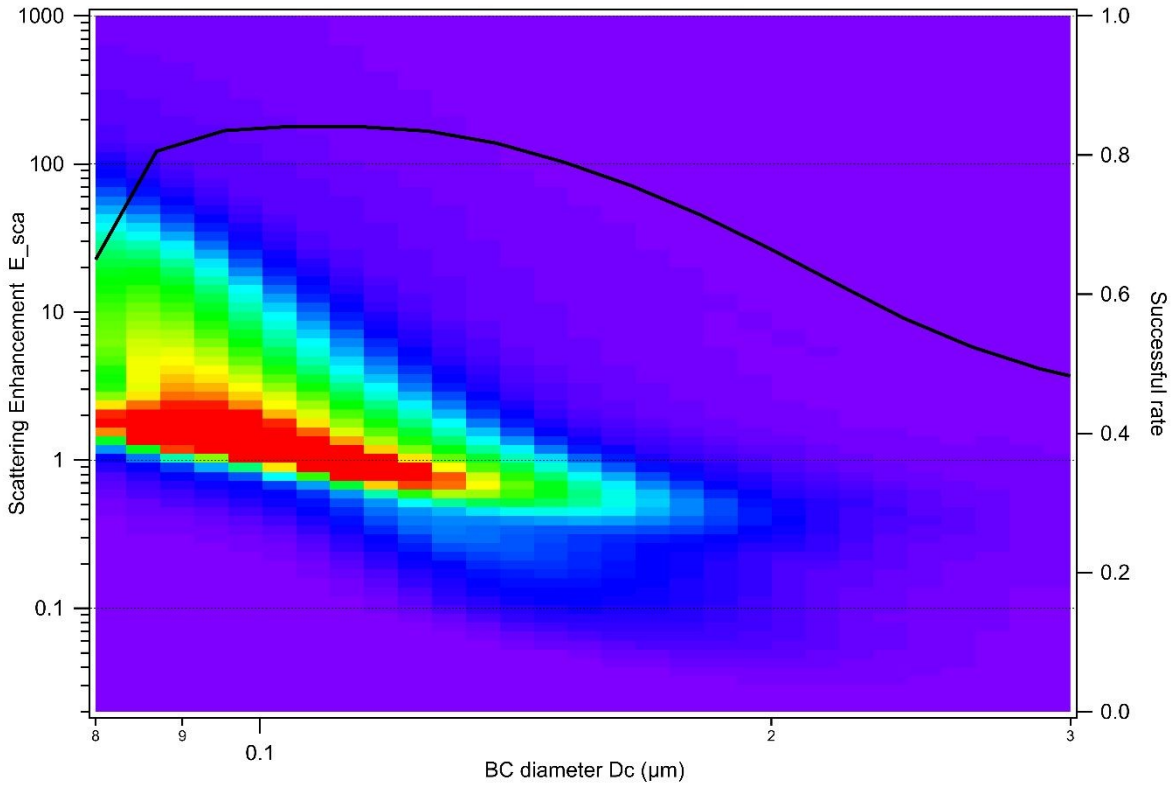

Figure 3: BT tower winter campaign Esca 2-D histogram. Larger Esca means thicker BC coating, Esca =1 means BC are not coated. The colour is set to red when the particle number density > 70% of the maximum.

Here, we applied scattering enhancement analysis [17, 23, 26, 28] to characterize the BC mixing state at BT Tower (Figure 3). Previous work identify four distinct mixing states which were not observed in this study [28]. BC observed at BT tower was primarily associated with thinly coated particles (Esca close to 1) across a broad range of BC core diameters (Dc). In contrast to the results for ground based measurement [23], BC in central London exhibited an absence of larger, thickly coated particles, implying limited biomass burning sources inside the footprint area. However, we cannot assert with complete confidence from Esca analysis that BC concentrations observed in this study is entirely not related with wood burning, as indicated from the successful rate in Figure 3. At the end of winter campaign, high peak concentrations of BC were identified (Figure S4) while ambient temperature and BLH were low. Which means convection can cause BC transport from rural areas, which may include BC from domestic burning sources. However, these BC concentrations have very limited effect on fluxes because of the low frequency and stable boundary layer corrections.

3.2 Micrometeorological conditions

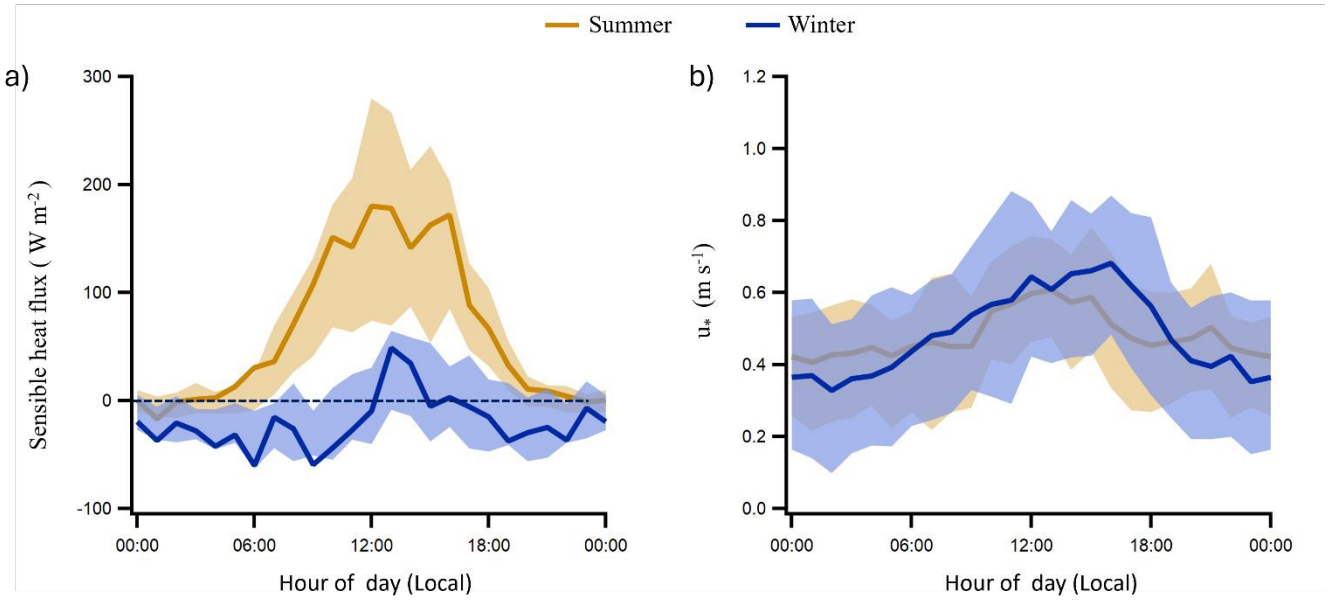

Figure 4: Sensible heat flux (a) and friction velocity (b) in summer (yellow) and winter (blue).

In EC measurements, u_* not only provides thresholds for advection flux, but also help us understand the diurnal cycle of turbulence development. The levels and diurnal patterns of u_* during winter (Figure 4b, blue) and summer (Figure 4b, yellow) exhibit similarities, suggesting that the measurement height is sufficient to minimize the impact of underlying surface roughness on the measurement results. Sensible heat flux (HF) represents the temperature difference between the upper and lower layers at the measurement site. In both winter (Figure 4a, yellow) and summer (Figure 4a, blue), HF increases rapidly after sunrise. This phenomenon is attributed to solar heating of the Earth's surface, leading to an elevation in the temperature of the lower layer. The near negative HF throughout the day in winter occurred due to weaker solar heating, resulting in slightly higher temperature of upper layer than lower layer. Solar heating during summer is more intense than in winter and heat the surface more efficiently, resulting in a greater temperature difference and positive HF.

3.3 BC fluxes

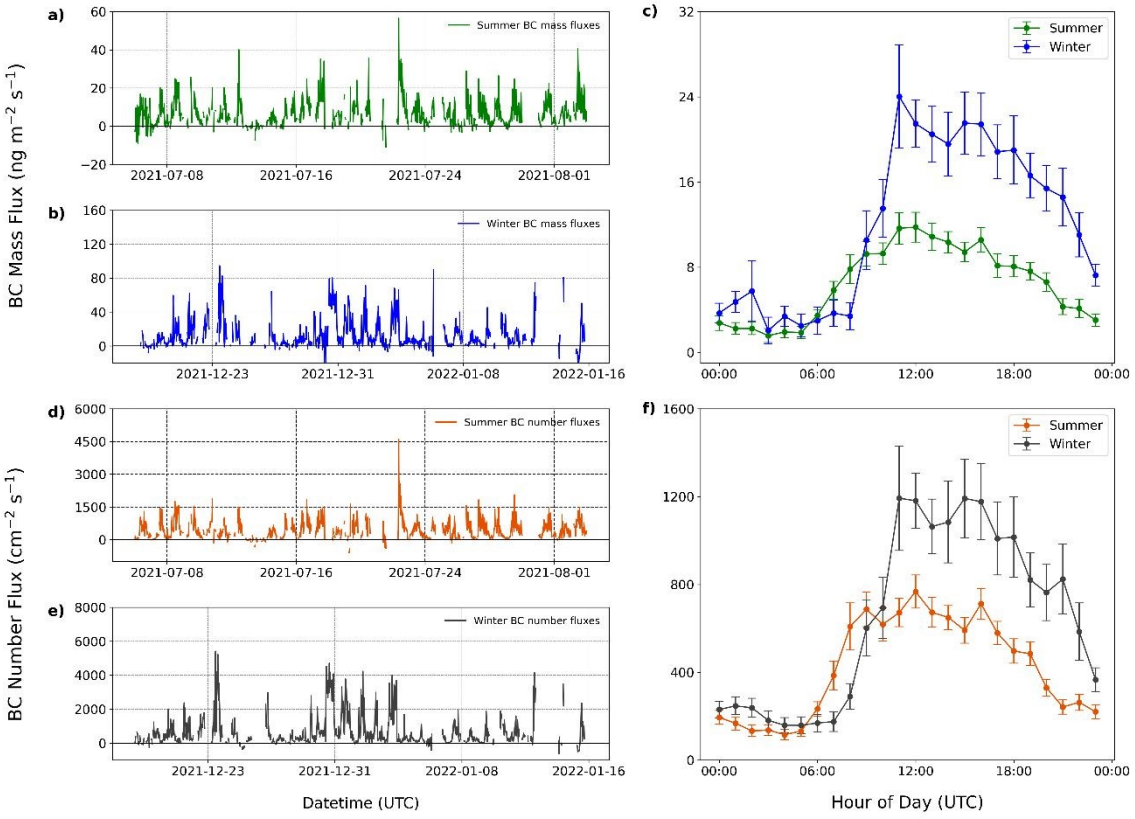

Figure 5: BT tower measured BC fluxes. BC mass fluxes in a) summer and b) winter, BC number fluxes in d) summer and e) winter. Diurnal profile of c) BC mass fluxes and f) number fluxes. Error bars in c) and f) are stand error.

		BC mass flux	BC number flux	BC mass concentration	BC number concentration
		ng m^{-2} s^{-1}	cm^{-2} s^{-1}	µg m^{-3}	cm^{-3}
Summer	**Mean**	6.826	442.5	0.2050	120.3
	Min	-10.89	-594.5	0.0008519	10.25
	Max	56.49	4613	0.6865	445.29
	Median	5.066	334.0	0.1701	99.40
	Standard Deviation	7.093	427.2	0.1325	77.51

	Number of points	929.0	943.0	1229	1229
Winter	**Mean**	13.25	686.6	0.3431	146.3
	Min	-22.35	-626.0	0.01726	12.06
	Max	199.6	9178	4.215	1955
	Median	7.265	343.2	0.2261	95.72
	Standard Deviation	17.61	950.3	0.4079	182.8
	Number of points	919.0	958.0	1327	1327

Table 1 BC number and mass fluxes and concentrations statistics in winter and summer. Calculated of the average of each 1-month campaign.

After applying the corrections and filter criteria described above, the remaining mass flux dataset comprised of in 919 (30-mintues) flux measurements remained for winter (Figure 5b) and 929 flux measurements for summer (Figure 5a). Overall, observations were dominated by positive BC fluxes, indicating the presence of anthropogenic activities producing BC emissions.

The average BC fluxes were higher during winter compared to summer (Table 1), which is also evident in the diurnal variation plots (Figure 5 c, f). In both seasons, BC fluxes rapidly increased after sunrise, peaked in the early afternoon, and gradually decreased after sunset. Furthermore, the diurnal patterns were similar between the two seasons, suggesting comparable emission sources for both periods. However, in the morning, summer fluxes rose earlier than winter due to a combination of reduced boundary layer mixing in the morning during winter and the impact of daylight-saving time changes.

Averaged BC mass concentrations were 0.34 μg m^{-3} in winter. This is a marked reduction to the 1.3 μg m^{-3} previously observed at an urban environment site in London in January 2012 [23]. From 2019 to 2022, the introduction of the ULEZ is estimated to have reduced the $PM_{2.5}$ emissions from cars and motorcycles, vans, taxis, HGVs and busses by 37%, 15%, 57%, 27% and 60% respectively [10]. Euro 6 restrictions for on road diesel vehicles were introduced in London from January 2014, which include the technological improvements by using improved Diesel Particle Filter (DPF). The change of Euro standards is estimated to have reduced on-road diesel BC emissions by 66% [9]. The 10-year BC concentrations decreased by 70% comparing to previous study [23], which follows the expectation of air quality policies and engine technical development in London.

3.4 Wind sector tends and spatial mapping

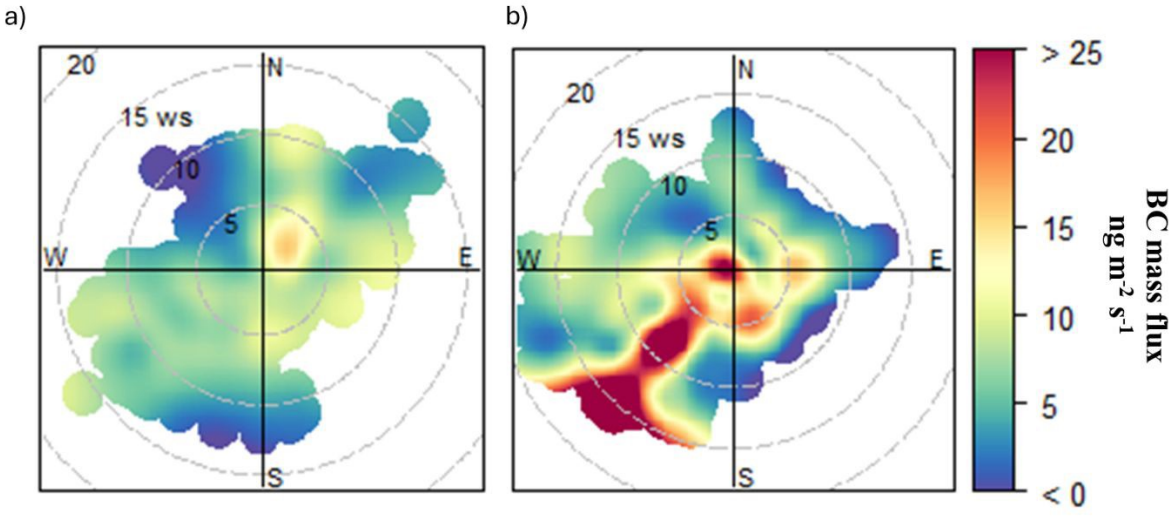

Figure 6: BC mass fluxes polar plots in a) summer and b) winter, as a function of wind speed.

An indicative identification of pollution source directions can be achieved using polar plots generated with the OpenAir package in R [44]. During the summer campaign (Figure 6a), the highest average BC emissions were associated with northeasterly winds. In contrast, during the winter (Figure 6b), a prominent point source was evident to the southwest, characterized by a clear band with an average mass flux >25 ng m^{-2} s^{-1}, which is also discernible in the footprint mapping plot (Figure 7b), indicating potential emission point sources. The highlighted emission area to the northeast of the BT tower in summer is near Euston railway station (CS1) as shown in Figure 7a. Other studies [35, 36] also reported NOx emissions from this area, attributed to the station supporting facilities in 2017, but these were no longer significant in 2021. However, we still attribute Euston station to BC emissions here, perhaps due to the construction site of High-Speed railway (HS2). Highlighted Sources in the winter spatial map are aligned to several areas including Euston station to the northeast, high traffic roads (Marylebone Road) to the west and point source to southwest. While NOx fluxes hotspot areas were collocated with this HS2 construction site during both campaigns as shown in Figure S11. However, the southwest point source attributes the most weighted to BC fluxes as shown in Figure S5 a. The dominant point source to southwest is aligned as some operating machinery and NRMM usage of construction sites inside the hotspot area (Figure 7b, CS2, CS3). CO fluxes hotspot areas were also collocated with these two construction sites to southwest in both campaigns (Figure S10). From the NRMM usage data provided by GLA, emissions with lower than EU stage IIIA NRMMs and construction machineries are still in use in Westminster and Camden borough [45].

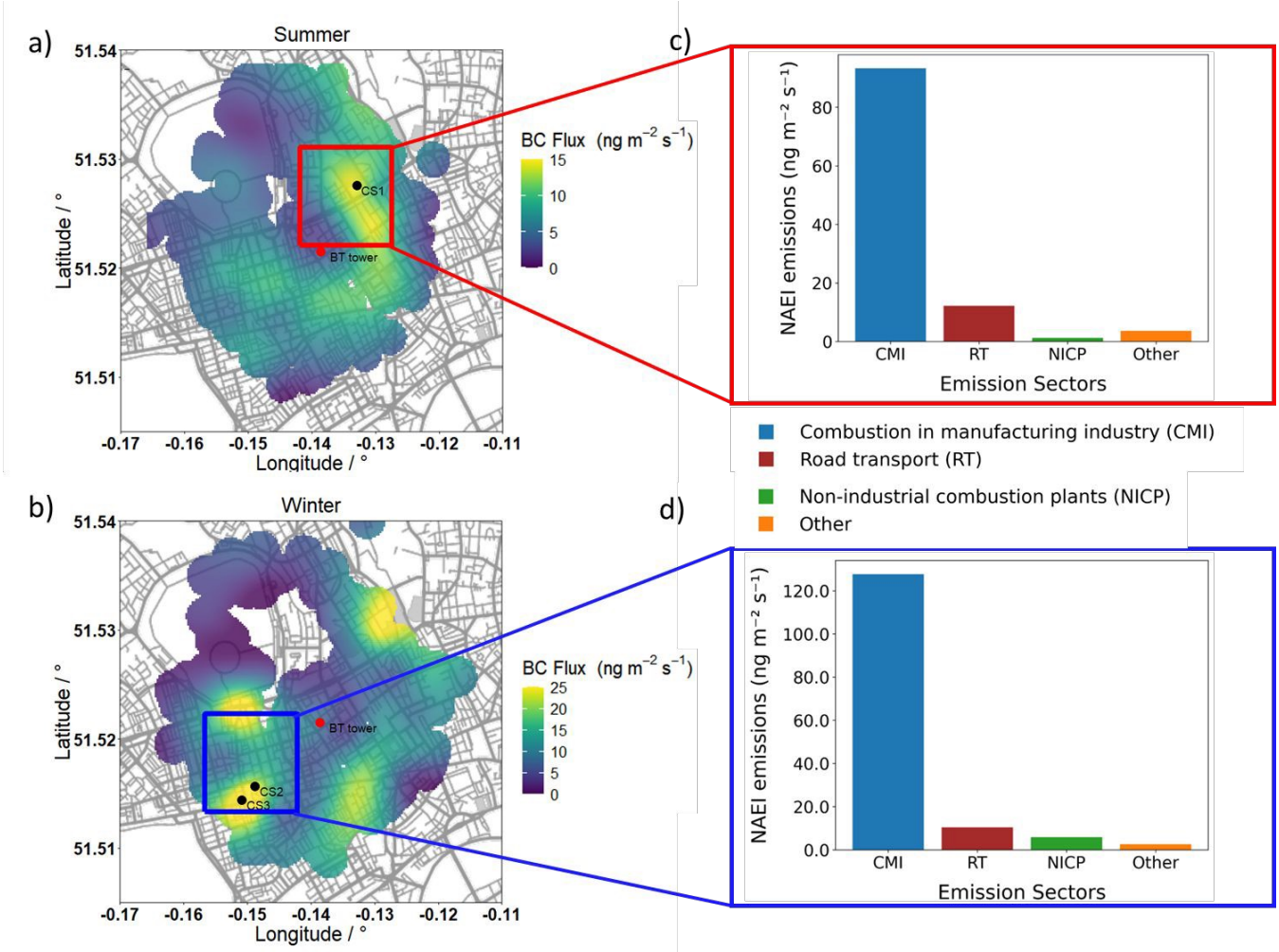

345 **Figure 7: Footprint spatial map in a) summer and b) winter with measurement site (BT tower) and potential Construction Sites (CS1, CS2, CS3) from construction information website [46] and Westminster City Council [47]. Together with NAEI grided emissions in c) Northeast (red frame) and d) Southwest (blue frame).**

3.5 Estimate of inventory emissions

NAEI [12] is an annual and comprehensive pollutant emissions estimate from 1970 to present. Emission sources are categorised
350 into 11 sectors, which are aggregated to United Nations Economic Commission for Europe (UNECE) Selected Nomenclature for reporting of Air Pollutants (SNAP), while large point emission sources are reported separately [48]. For each sector, a national total emission is calculated using activity statistics data and emission rates for the pollutant emitted from the source of interest (emission factor). Spatially resolved 1 km × 1 km gridded and spatially resolved modelled estimates of NAEI emissions, including point source and area source, are provided as emission maps [48]. Two gridded areas were selected based on the major
355 BC footprint from the NAEI spatial map, and the emissions were converted to the same unit as observed emissions (ng m^{-2} s^{-1}). The key source of BC emissions identified by the NAEI is Combustion in Manufactory Industry (CMI), which accounts for

85% (SW) and 83% (NE) of the total BC emissions, respectively (Figure 7 c, d). While Road transport (RT), Non-industrial combustion plant and other sources account for 15% (SW) and 17% (NE). In the NAEI, the CMI sector is directed to manufacturing industries and construction reporting as Nomenclature for Reporting (NFR) 1A2, which includes 8 NFR categories and subdivided in 21 NAEI categories shown in Table 3-6 and 3-7 of NAEI report [49]. In the NAEI 2021, construction NRMM(1.A.2.g.vii, hereafter referred as NRMM) used by construction is estimated to contribute 11.4% which is the second largest category in CMI sector [13]. As discussed in Section 2.1, the footprint area is not expected to include manufacturing industries except construction sites as the surroundings of BT tower are high-density commercial areas. Therefore, dominant BC emission source in footprint area by observation and inventory estimation is in good agreement with respect to which construction is significant.

However, CMI emissions are estimated by the NAEI to be larger than 120 ng m^{-2} s^{-1} in winter (southwest) and > 80 ng m^{-2} s^{-1} in summer (northeast), while observed BC emissions to be 25 ng m^{-2} s^{-1} in winter and 15 ng m^{-2} s^{-1} in summer in hotspot area (Figure 7 a, b and Figure S7). Road transport (RT) is estimated by the NAEI to be the second largest BC source in the footprint area, the NAEI emissions amount matches observed emission in non-highlighted areas in Figure 7, which are both around 10 ng m^{-2} s^{-1}.

Additionally, gridded NAEI BC emissions were also normalised to NOx and CO to provide more comparable results. The NAEI emission ratio across all sectors of BC/NOx (0.021 to SW, 0.018 to NE) is around 3.2 and 3.5 times larger than the observed ratios in winter and summer (Figure 8 c, a) while BC/CO (0.035 to SW, 0.048 to NE) ratios were 32.4 and 12.5 times larger than observations in winter and summer (Figure 8 d, b). Comparing the total emissions and ratios between NAEI and observations, the overestimate in the NAEI may mainly come from CMI sectors rather than RT.

Better agreements are found after removing CMI sector, NAEI BC to be 23 ng m^{-2} s^{-1} (SW) and 19 ng m^{-2} s^{-1} (NE). BC/NOx (0.012 to SW, 0.010 to NE) ratios were 1.9 and 2.1 times larger than observations, while BC/CO (0.006833 to SW and 0.013 to NE) ratios were 2.4 and 10 times larger than observations. CMI emission are calculated using fuel consumption data from UK statistics (DUKES) and default emission factor from European Environment Agency (EEA) by NAEI Tier 3 methodology which includes complex model approaches to provide accuracy estimation [49]. Construction NRMM emission estimation in NAEI uses EEA default BC emission factor which represent global average performance rather than accuracy UK circumstances. Furthermore, construction sites are not identified as BC point sources in the NAEI even if they make a significant contribution. Even Off-road emissions are spatial to the map using revised employment statistics [48] which removes some cases in urban area, NRMM emissions are still overestimated in NAEI 2021. However, the highly episodic and spatially granularity of construction sites would also make the estimation to be difficult.

3.6 Comparisons with other fluxes

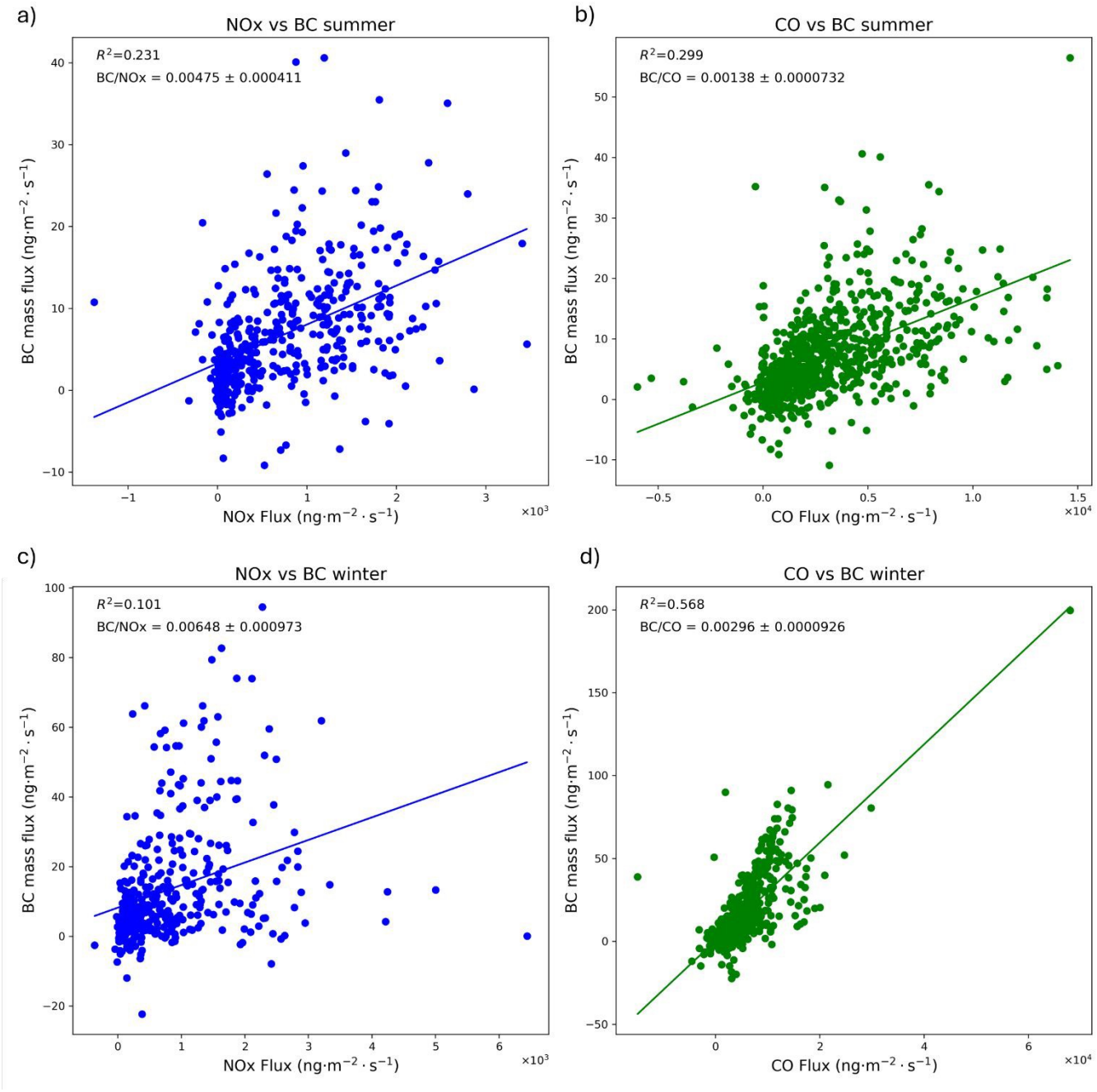

Figure 8: NOx flux [35] with BC mass flux in a) summer and c) winter and CO with BC mass flux in b) summer and d) winter. Uncertainties on the BC/NOx and BC/CO ratios are standard deviation.

Other pollutants may be co-emitted with BC from the sources. NOx and CO were selected for comparison with BC because of their significant contributions to construction and road transport [30, 50]. The orthogonal distance regression linear correlations of BC, NOx and CO are shown in Figure 8. Low correlations between BC and NOx in summer ($R^2 = 0.23$) and winter ($R^2 = 0.10$) is likely due to the prominence of gas combustion in boilers which now dominate NOx emissions in central London [35]. This combustion is much cleaner and has much lower BC emissions compared to other sources like diesel internal combustion engines.

A stronger correlation between BC and CO in winter ($R^2 = 0.57$) and summer ($R^2 = 0.30$) suggests that these pollutants are co-emitted in central London. Road transport and Other mobile machinery are estimated by NAEI to be the most contribution to CO emissions around BT tower. With the introduction of Euro 6 diesel engines and ULEZ policy, as well as the proliferation of electric vehicles, BC emissions from road transport is less obvious. Therefore, the BC and CO correlation gives confidence that construction NRMM is the highlighted source of BC.

Winter BC mass fluxes were observed to be 48% larger than those in summer. Similarly, Winter BC/NOx and BC/CO ratios were 27% and 53% higher, respectively, compared to summer. These differences may be attributed to reduced industrial and traffic emissions during the COVID-19 pandemic affecting the summer period, but equally also to additional winter sources such as from heating and vehicle cold starts. The representative construction activities around BT tower rose by 22% in the winter campaign period compared to the summer [45]. While the representative traffic flow in winter was 3.7% smaller than summer [35]. The rise in BC/NOx ratios aligns with the 22% increase in construction activity. While the rise in BC/CO is likely influenced by cold start in winter, contributing to the 53% increase. Consequently, differences in BC emissions between winter and summer appear to be driven by a combination of changes in construction and traffic activities.

UK follows EEA regulation system for non-road machinery emission controls, which is covering major pollutants including NOx, CO, PM and Hydrocarbons [51]. The EEA emission standards include BC/$PM_{2.5}$ emission ratios by engine types and power ratings. To better understand construction NRMM contributions to BC emissions, BC/CO and BC/NOx ratios were calculated from non-road machinery EEA regulations (Table 2). Given that NOx and BC are not co-emitted from gas combustion to the Northeast of BT tower, we selected Southwest BC/NOx ratio which is more related ($R^2 = 0.28$ in summer, R^2=0.27 in winter) to BC (Figure S8 a, b) to compare with EEA NRMM standard. Comparing the ratios measured from the BT tower as shown in Figure 8, we find good agreement for EU stage IIIB, IV (no DPF) and V which matching the requirements of ULEZ NRMM standards [52].

Non-road diesel			
EU Stage	**Engine size**	**BC/CO**	**BC/NOx**
Stage I	**Power rate (P, kWh)**		
A	130<= P<560	0.0756	0.0411
B	75<=P<130	0.112	0.0609
C	37<=P<75	0.105	0.739

Stage II			
D	18<=P<37	0.116	0.080
E	130<=P<560	0.0400	0.233
F	75<=P<130	0.0480	0.0400
G	37<=P<75	0.0640	0.0457
Stage IIIA			
H	130<=P<560	0.0400	\
I	75<=P<130	0.0480	\
J	37<=P<75	0.0640	\
K	19<=P<37	0.0873	\
Stage IIIB, no DPF			
L	130<=P<560	0.00500	0.00875
M	75<=P<130	0.00350	0.00530
N	56<=P<75	0.00350	0.00530
P	37<=P<56	0.00350	\
Stage IIIB, DPF			
L	130<=P<560	0.00107	0.001875
M	75<=P<130	0.000750	0.00114
N	56<=P<75	0.000750	0.00114
P	37<=P<56	0.000750	\
Stage IV, no DPF			
Q	130<=P<560	0.00500	0.0438
R	56<=P<130	0.00350	0.0438
Stage IV, DPF			
Q	130<=P<560	0.00107	0.00938
R	56<=P<130	0.000750	0.00938
Stage V			
NRE-v/c-7	P>560	0.00193	0.00193
NRE-v/c-6	130≤P≤560	0.000429	0.00563
NRE-v/c-5	56≤P<130	0.000450	0.00563
NRE-v/c-4	37≤P<56	0.000450	\
NRE-v/c-3	19≤P<37	0.000450	\
NRE-v/c-2	8≤P<19	0.00909	\

NRE-v/c-1	P<8	0.00750	\
Generators	P>560	0.00784	0.00150
Observations			
Winter		0.00296 ± 0.0000926 (total)	0.00648± 0.000973 (total) 0.0168 ±0.00181 (SW)
Summer		0.00138 ± 0.0000732 (total)	0.00475± 0.000471 (total) 0.00536 ± 0.000609 (SW)

Table 2: Non-road machinery (1A2.gvii) emission standard with EU stage I to V BC/CO and BC/NOx ratios [51] , comparing with BT tower observations. From Stage IIIB, diesel particle filters (DPF) are applied to the engine. The "EU Stage" column indicates engine categories (EU stage I to V), with sub-categories denoted by letters A to R for EU stage I to IV, and by codes c-1 to c-7 for non-road engine (NRE) at EU stage V, reflecting different power rate bands. Generator is shown as a distinct sub-category in EU stage V. Engine power rate (P) bands are shown in column "Engine size" with unit of kWh. BC/CO and BC/NOx columns represent the ratios of EU standard categories and observations. Front slash ("/") denotes no data. Observed BC/CO ratios correspond to the total footprint area, while observed BC/NOx ratios are reported separately for the total footprint and southwest areas. Observed ratios include mean values and standard deviation from each measurement campaign.

However, in the footprint area the policy for NRMM emission control lags behind those for road vehicles standards level (e.g. ULEZ), and that is likely the reason why construction BC emissions stand out. The GLA pledged to develop nearly 60000 jobs and 50000 housing in London after becoming one of the largest landowners [53]. Large generators and NRMM operating at construction sites significantly contribute to air pollution, accounting for 34% of PM_{10} and 14% of $PM_{2.5}$, which are the largest and second-largest source in London, respectively [50, 54]. NRMM and generator registration data provided by GLA for the Westminster and Camden boroughs reveal evidence of high-power-rate machinery usage (greater than 130 kWh) around the BT tower during both campaign periods. Although time series on machinery usage for specific sites cannot be examined, the evidence above is substantial enough to raise concerns about BC emissions from the construction industry in central London. Similar concerns regarding gas and particulate pollutants from NRMM have been raised [50]. GLA also has future plans in London for NRMM emission control in the ULEZ to meet Stage IV by 2025 and Stage V by 2030, as well as zero emissions by 2040 [52]. Consequently, it is imperative to continuously emphasise the importance of this sector for BC emissions, and to address the uncertainties in inventory estimates for construction activities in the coming years. National strategies and policies, such as Industrial decarbonisation strategy [55], will require further infrastructure development, potentially increasing emissions from NRMM sources if not effectively regulated.

3.7 Comparisons with other cities

Previous studies conducted observations of BC fluxes from a tower (102 m) in Beijing[17] during the winter of 2016 (mean 5.49 ng m^{-2} s^{-1}) and the summer of 2017 (mean 6.10 ng m^{-2} s^{-1}), and in Delhi [19] from a 35 m tower during November 2018 (mean 25.8 ng m^{-2} s^{-1}). All fluxes are whole campaign average. In the studies of these three cities, emission inventories are overestimating BC emissions in urban areas. BC fluxes in London form this study were similar to fluxes in Beijing in summer,

and twice larger than Beijing in winter, while 3.5 (summer) and 2.0 (winter) times lower than in Delhi. During observations in the 3 cities, London had introduced Euro 6 for on road vehicles, while Beijing was on China 5 (Euro 5) controls, while Delhi was on Bharat Stage IV (Euro 4) standard. Moreover, Beijing and Delhi diesel powered vehicles were only allowed during night-time and Beijing's vehicle fleet was ahead in terms of electrification. Thus, direct comparison between urban flux measurement datasets needs to be treated with caution due to differences in local emission controls[56, 57], but also in site characteristics [58]. Some measurements might be located in more intensely urban than others, while meteorological conditions would also different[59, 60]. To eliminate this latter effect, Beijing BC fluxes normalised by NOx and CO [17] for comparison to evaluate traffic and construction BC emissions. While Delhi BC fluxes [19], NOx and CO fluxes [61] are retrieved for corresponding comparisons. Due to Bharat Stage IV (Euro 4) was used as on-road vehicles emissions, BC emissions were thought to have been dominated by road traffic in Delhi.

Seasons	Location	BC number flux mean (cm^{-2} s^{-1})	BC mass flux mean (ng m^{-2} s^{-1})	BC/NOx	BC/CO
Summer	Beijing	334.37	6.10	0.0052	0.0011
	London	442.50	6.83	0.0048± 0.00047	0.0014 ±0.000073
Winter	Beijing	261.25	5.49	0.0058	0.0007
	London	686.60	13.3	0.0065± 0.00097	0.0030 ±0.000093
Post-monsoon	Delhi	850.00	25.8	0.0011± 0.00089	0.00036 ± 0.00065

Table 3: Observations of averaged BC number and mass fluxes. And BC/NOx, BC/CO ratios in Beijing, and London and Delhi (with standard deviation).

The primary source for BC emissions in Beijing was attributable to gasoline traffic contributions accounting for 92% of the total flux [17]. We are not aware of any major construction sites operating inside footprint area during the Beijing measurements. For traffic control, Beijing has banned diesel vehicles entry during daytime, leading to BC emissions in lower than London even under China 5 (Euro 5) standard. However, the BC concentrations in Beijing are much higher than in London, which may be due to transportation from wider north plain or rural area, or limited diffusion condition due to shallow boundary layer. This increases the concerns of both construction contribution and traffic control policy to BC emissions in London ULEZ area. Normalised Summer BC emissions have no significant difference in Beijing and London, which is due to low human activities (especially less construction sites operation) during COVID pandemic in London. The London winter BC/CO flux ratio was

four times larger than in Beijing, indicating additional non-gasoline BC sources in London. Cold starts in Beijing leading to high CO emissions could also be the potential reason for low BC/CO ratios. The London BC/NOx flux ratio was 4.4 times (summer) and 5.9 times (winter) larger than in Delhi. The potential reason could be night-time NO storage leading to high NOx emissions in day-time when nighttime boundary layer collapse [62]. The Delhi BC/CO ratio has large uncertainty due to lack of matched data points (53 matched data points). However, bearing in mind the uncertainties in the correlations, the comparable agreement of normalized BC emissions between Beijing and London nevertheless enhances confidence in quantifying urban BC emissions using EC fluxes.

4 Conclusion

In this study, BC emissions in central London during two different seasons were quantified using the eddy covariance technique. We found that BC mass and number fluxes in winter (13.3 ng m^{-2} s^{-1}, 687 cm^{-2} s^{-1}) were approximately twice as high as those in summer (6.83 ng m^{-2} s^{-1}, 443 cm^{-2} s^{-1}) due to increased construction sites resulting from increasing human activities after COVID. Thick BC coatings were absent compared to earlier measurements in 2012, indicating traffic associated BC emissions dominant in central London rather than biomass burning. Footprint analysis highlighted BC emission sources were collocated with construction sites. Comparisons with the spatially resolved NAEI revealed that the construction sector is the dominant source of BC emissions in footprint area. Quantitatively, the measured emissions agreed well with the NAEI for most sources, but construction was overestimated in the NAEI by a factor of 5-6 compared to the observations due to less representative emission factor and spatial data use. However, it is recognised that quantitatively accounting for source within inventories is extremely challenging due to its spatial granularity and highly episodic. Comparisons of BC/NOx and BC/CO ratios with EEA emission standards raises additional concerns for large machinery used in the construction industry. It is encouraged to increase the spatial coverage of BC measurements for better identifying hotspots in urban emissions study in the future.

BC concentrations in London have significantly decreased since the introduction of the ULEZ and the use of more efficient diesel particle filters in Euro 6 road diesel vehicles. However, to meet the WHO guidelines for urban air quality and address human health concerns, air quality in London can be further improved by introducing tightened regulation for NRMM. The conclusions from this study also highlight concerns about NRMM in other countries with high construction demands.

Competing interests

The authors declare no conflict of interest.

Code availability

The EddyPro software to generate fluxes and 1-D footprint can be freely download at https://www.licor.com/support/EddyPro/software.html. The R package Openair used to generate polar plots and spatial flux footprint on map can be freely accessed at https://github.com/openair-project/openair.

Data availability

NAEI data for Figure 7 has been taken from National Atmospheric Emission Inventory website (https://naei.energysecurity.gov.uk/).

The ERA5 boundary layer height data can be accessed at http://cds.climate.copernicus.eu/cdsapp#!/home.

The construction operation data used in this study were provided by GLA from freedom of information at (https://www.london.gov.uk/programmes-and-strategies/environment-and-climate-change/pollution-and-air-quality/nrmm).

The processed BC fluxes data are available on Centre for Environmental Data Analysis Archive (https://catalogue.ceda.ac.uk/uuid/ab605b618884401c91afd0274c92144e/).

Author contributions

ZC made BC measurements, calculated the fluxes, performed footprint modelling and analysed the data. ZC wrote the paper and produced the figures. JA, MF, EN, JC provided support with the measurements from sites. JA, DH, DL, RJ provided support with the SP2 data processing. DH provided training on SP2 toolkits software. JA, EN, BL, CH, RJ provided support with the flux calculations. BL and CH provided meteorological data and explanation. WD provided support with footprint modelling and the codes. CH provided CO fluxes data. SC provided NOx fluxes data and traffic activities data. All authors read and commented the paper.

Acknowledgements

The authors thank Neil Mullinger (UK Centre for Ecology and Hydrology) for instrument and sample line maintenance; and BT for granting use for BT Tower for research. The authors also thank Carl Desouza and David Green (Imperial College London) for guidance to locate construction operation data.

Financial support

This work was funded by UKRI through the OSCA project (grant refs NE/T001984/1 and NE/T001798/2), part of the NERC Clean Air Strategic Priorities Fund. The BT Tower Atmospheric Observatory is supported by NERC through the UKCEH National Capability for UK Challenges Programme - NE/Y006208/1.

References

1. WHO, World Health Organisation Ambient (outdoor) air pollution, https://www.who.int/news-room/fact-sheets/detail/ambient-(outdoor)-air-quality-and-health).
2. T. C. Bond, S. J. Doherty, D. W. Fahey, P. M. Forster, T. Berntsen, B. J. Deangelo, M. G. Flanner, S. Ghan, B. Kärcher, D. Koch, S. Kinne, Y. Kondo, P. K. Quinn, M. C. Sarofim, M. G. Schultz, M. Schulz, C. Venkataraman, H. Zhang, S. Zhang, N. Bellouin, S. K. Guttikunda, P. K. Hopke, M. Z. Jacobson, J. W. Kaiser, Z. Klimont, U. Lohmann, J. P. Schwarz, D. Shindell, T. Storelvmo, S. G. Warren and C. S. Zender, Bounding the role of black carbon in the climate system: A scientific assessment, *Journal of Geophysical Research Atmospheres*, 2013, **118**, 5380-5552.
3. E. J. Highwood and R. P. Kinnersley, When smoke gets in our eyes: The multiple impacts of atmospheric black carbon on climate, air quality and health, *Environment International*, 2006, **32**, 560-566.
4. J. L. Nichols, E. O. Owens, S. J. Dutton and T. J. Luben, Systematic review of the effects of black carbon on cardiovascular disease among individuals with pre-existing disease, *International Journal of Public Health*, 2013, **58**, 707-724.
5. W. J. Gauderman, E. Avol, F. Gilliland, H. Vora, D. Thomas, K. Berhane, R. McConnell, N. Kuenzli, F. Lurmann, E. Rappaport, H. Margolis, D. Bates and J. Peters, The Effect of Air Pollution on Lung Development from 10 to 18 Years of Age, *New England Journal of Medicine*, 2004, **351**, 1057-1067.
6. WHO, WHO global air quality guidelines: particulate matter (PM2.5 and PM10), ozone, nitrogen dioxide, sulfur dioxide and carbon monoxide.*Journal*, 2021.
7. United Nations Environment Programme UNEP and W. M. O. WMO, *Integrated Assessment of Black Carbon and Tropospheric Ozone*, 2011.
8. GLA, Expanded Ultra Low Emission Zone - First Month Report | London City Hall, https://www.london.gov.uk/programmes-and-strategies/environment-and-climate-change/environment-publications/expanded-ultra-low-emission-zone-first-month-report).
9. L. Ntziachristos and Z. Samaras, *EMEP/EEA air pollutant emission inventory guidebook 2023*, 2023.
10. GLA, Inner London Ultra Low Emission Zone Expansion One Year Report | London City Hall, https://www.london.gov.uk/programmes-strategies/environment-and-climate-change/environment-and-climate-change-publications/inner-london-ultra-low-emission-zone-expansion-one-year-report#background-165719-title).
11. J. D. Lee, C. Helfter, R. M. Purvis, S. D. Beevers, D. C. Carslaw, A. C. Lewis, S. J. Møller, A. Tremper, A. Vaughan and E. G. Nemitz, Measurement of NOx Fluxes from a Tall Tower in Central London, UK and Comparison with Emissions Inventories, *Environmental Science & Technology*, 2015, **49**, 1025-1034.
12. NAEI, NAEI, UK National Atmospheric Emissions Inventory - NAEI, UK, https://naei.beis.gov.uk/).
13. NAEI, *UK Spatial Emissions Methodology A report of the National Atmospheric Emission Inventory 2020*, 2022.
14. U. Paliwal, M. Sharma and J. F. Burkhart, Monthly and spatially resolved black carbon emission inventory of India: uncertainty analysis, *Atmospheric Chemistry and Physics*, 2016, **16**, 12457-12476.
15. H. Simon, D. T. Allen and A. E. Wittig, Fine Particulate Matter Emissions Inventories: Comparisons of Emissions Estimates with Observations from Recent Field Programs, *Journal of the Air & Waste Management Association*, 2008, **58**, 320-343.

16. E. Nemitz, J. L. Jimenez, J. A. Huffman, I. M. Ulbrich, M. R. Canagaratna, D. R. Worsnop and A. B. Guenther, An Eddy-Covariance System for the Measurement of Surface/Atmosphere Exchange Fluxes of Submicron Aerosol Chemical Species—First Application Above an Urban Area, *Aerosol Science and Technology*, 2008, **42**, 636-657.
17. R. Joshi, D. Liu, E. Nemitz, B. Langford, N. Mullinger, F. Squires, J. Lee, Y. Wu, X. Pan, P. Fu, S. Kotthaus, S. Grimmond, Q. Zhang, R. Wu, O. Wild, M. Flynn, H. Coe and J. Allan, Direct measurements of black carbon fluxes in central Beijing using the eddy covariance method, *Atmospheric Chemistry and Physics*, 2021, **21**, 147-162.
18. E. W. Emerson, J. M. Katich, J. P. Schwarz, G. R. McMeeking and D. K. Farmer, Direct Measurements of Dry and Wet Deposition of Black Carbon Over a Grassland, *Journal of Geophysical Research: Atmospheres*, 2018, **123**, 12, 212-277, 290.
19. R. Joshi, Black carbon flux measurements in megacities using the eddy covariance method.*Journal*, 2021.
20. S. E. Lane, J. F. Barlow and C. R. Wood, An assessment of a three-beam Doppler lidar wind profiling method for use in urban areas, *Journal of Wind Engineering and Industrial Aerodynamics*, 2013, **119**, 53-59.
21. R. S. Gao, J. P. Schwarz, K. K. Kelly, D. W. Fahey, L. A. Watts, T. L. Thompson, J. R. Spackman, J. G. Slowik, E. S. Cross, J. H. Han, P. Davidovits, T. B. Onasch and D. R. Worsnop, A Novel Method for Estimating Light-Scattering Properties of Soot Aerosols Using a Modified Single-Particle Soot Photometer, *Aerosol Science and Technology*, 2007, **41**, 125-135.
22. H. A. Michelsen, C. Schulz, G. J. Smallwood and S. Will, Laser-induced incandescence: Particulate diagnostics for combustion, atmospheric, and industrial applications, *Progress in Energy and Combustion Science*, 2015, **51**, 2-48.
23. D. Liu, J. D. Allan, D. E. Young, H. Coe, D. Beddows, Z. L. Fleming, M. J. Flynn, M. W. Gallagher, R. M. Harrison, J. Lee, A. S. H. Prevot, J. W. Taylor, J. Yin, P. I. Williams and P. Zotter, Size distribution, mixing state and source apportionment of black carbon aerosol in London during wintertime, *Atmos. Chem. Phys.*, 2014, **14**, 10061-10084.
24. M. Laborde, M. Schnaiter, C. Linke, H. Saathoff, K. H. Naumann, O. Möhler, S. Berlenz, U. Wagner, J. W. Taylor, D. Liu, M. Flynn, J. D. Allan, H. Coe, K. Heimerl, F. Dahlkötter, B. Weinzierl, A. G. Wollny, M. Zanatta, J. Cozic, P. Laj, R. Hitzenberger, J. P. Schwarz and M. Gysel, Single Particle Soot Photometer intercomparison at the AIDA chamber, *Atmos. Meas. Tech.*, 2012, **5**, 3077-3097.
25. D. Liu, J. Whitehead, M. R. Alfarra, E. Reyes-Villegas, Dominick V. Spracklen, Carly L. Reddington, S. Kong, Paul I. Williams, Y.-C. Ting, S. Haslett, Jonathan W. Taylor, Michael J. Flynn, William T. Morgan, G. McFiggans, H. Coe and James D. Allan, Black-carbon absorption enhancement in the atmosphere determined by particle mixing state, *Nature Geoscience*, 2017, **10**, 184-188.
26. J. W. Taylor, J. D. Allan, D. Liu, M. Flynn, R. Weber, X. Zhang, B. L. Lefer, N. Grossberg, J. Flynn and H. Coe, Assessment of the sensitivity of core / shell parameters derived using the single-particle soot photometer to density and refractive index, *Atmos. Meas. Tech.*, 2015, **8**, 1701-1718.
27. N. Moteki, Y. Kondo and S.-i. Nakamura, Method to measure refractive indices of small nonspherical particles: Application to black carbon particles, *Journal of Aerosol Science*, 2010, **41**, 513-521.
28. D. Liu, R. Joshi, J. Wang, C. Yu, J. D. Allan, H. Coe, M. J. Flynn, C. Xie, J. Lee, F. Squires, S. Kotthaus, S. Grimmond, X. Ge, Y. Sun and P. Fu, Contrasting physical properties of black carbon in urban Beijing between winter and summer, *Atmos. Chem. Phys.*, 2019, **19**, 6749-6769.
29. T. Foken, M. Aubinet and R. Leuning, in *Eddy Covariance: A Practical Guide to Measurement and Data Analysis*, eds. M. Aubinet, T. Vesala and D. Papale, Springer Netherlands, Dordrecht, 2012, DOI: 10.1007/978-94-007-2351-1_1, pp. 1-19.
30. C. Helfter, A. H. Tremper, C. H. Halios, S. Kotthaus, A. Bjorkegren, C. S. B. Grimmond, J. F. Barlow and E. Nemitz, Spatial and temporal variability of urban fluxes of methane, carbon monoxide and carbon dioxide above London, UK, *Atmos. Chem. Phys.*, 2016, **16**, 10543-10557.
31. B. Langford, P. K. Misztal, E. Nemitz, B. Davison, C. Helfter, T. A. M. Pugh, A. R. MacKenzie, S. F. Lim and C. N. Hewitt, Fluxes and concentrations of volatile organic compounds from a South-East Asian tropical rainforest, *Atmos. Chem. Phys.*, 2010, **10**, 8391-8412.
32. G. Burba, *Eddy Covariance Method for Scientific, Regulatory, and Commercial Applications*, 2022.
33. D. Vickers and L. Mahrt, Quality Control and Flux Sampling Problems for Tower and Aircraft Data, *Journal of Atmospheric and Oceanic Technology*, 1997, **14**, 512-526.

34. T. Foken, in *Micrometeorology*, ed. T. Foken, Springer Berlin Heidelberg, Berlin, Heidelberg, 2017, DOI: 10.1007/978-3-642-25440-6_4, pp. 143-205.
35. S. J. Cliff, W. Drysdale, J. D. Lee, C. Helfter, E. Nemitz, S. Metzger and J. F. Barlow, Pandemic restrictions in 2020 highlight the significance of non-road NO_x sources in central London, *Atmospheric Chemistry and Physics*, 2023, **23**, 2315-2330.
36. W. S. Drysdale, A. R. Vaughan, F. A. Squires, S. J. Cliff, S. Metzger, D. Durden, N. Pingintha-Durden, C. Helfter, E. Nemitz, C. S. B. Grimmond, J. Barlow, S. Beevers, G. Stewart, D. Dajnak, R. M. Purvis and J. D. Lee, Eddy covariance measurements highlight sources of nitrogen oxide emissions missing from inventories for central London, *Atmospheric Chemistry and Physics*, 2022, **22**, 9413-9433.
37. J. M. Wilczak, S. P. Oncley and S. A. Stage, Sonic Anemometer Tilt Correction Algorithms, *Boundary-Layer Meteorology*, 2001, **99**, 127-150.
38. J. H. C. Gash and A. D. Culf, Applying a linear detrend to eddy correlation data in realtime, *Boundary-Layer Meteorology*, 1996, **79**, 301-306.
39. M. Mauder and T. Foken, Impact of post-field data processing on eddy covariance flux estimates and energy balance closure, *Meteorologische Zeitschrift*, 2006, **15**, 597-609.
40. J. C. Kaimal and J. J. Finnigan, *Atmospheric boundary layer flows: their structure and measurement*, Oxford university press, 1994.
41. S. P. Oncley, C. A. Friehe, J. C. Larue, J. A. Businger, E. C. Itsweire and S. S. Chang, Surface-layer fluxes, profiles, and turbulence measurements over uniform terrain under near-neutral conditions, *Journal of Atmospheric Sciences*, 1996, **53**, 1029-1044.
42. R. L. Desjardins, J. I. Macpherson, P. H. Schuepp and F. Karanja, in *Boundary Layer Studies and Applications: A Special Issue of Boundary-Layer Meteorology in honor of Dr. Hans A. Panofsky (1917–1988)*, ed. R. E. Munn, Springer Netherlands, Dordrecht, 1989, DOI: 10.1007/978-94-009-0975-5_5, pp. 55-69.
43. N. Kljun, P. Calanca, M. W. Rotach and H. P. Schmid, A Simple Parameterisation for Flux Footprint Predictions, *Boundary-Layer Meteorology*, 2004, **112**, 503-523.
44. D. C. Carslaw and K. Ropkins, openair — An R package for air quality data analysis, *Environmental Modelling & Software*, 2012, **27-28**, 52-61.
45. GLA, Greater London Authority construction sites.*Journal*, 2023.
46. Considerate Constructors Scheme, Construction Map, https://www.constructionmap.info/, (accessed 2021/12/17).
47. WCC, Westminster City Council, https://www.westminster.gov.uk/, (accessed 2024/05/20, 2024).
48. I. Tsagatakis, J. Richardson, C. Evangelides, M. Pizzolato, B. Richmond, S.-M. Hows, B. Pearson, N. Passant, M. Pommier and A. Otto, *UK Spatial Emissions Methodology: A report of the National Atmospheric Emission Inventory 2021*, 2023.
49. M. Elliott, D. Ingledew, B. Richmond, S. Del Vento, S. Gorji, N. Hamilton, E. Karagianni, A. Kelsall, Y. Pang, N. Passant, B. Pearson, J. Richardson, R. Stewart, G. Thistlethwaite, I. Tsagatakis, D. Wakeling, J. Wiltshire, J. Wong, M. Hobson, A. Carswell, U. Dragosits and S. Anthony, *UK Informative Inventory Report (1990 to 2022)*, 2024.
50. C. D. Desouza, D. J. Marsh, S. D. Beevers, N. Molden and D. C. Green, Real-world emissions from non-road mobile machinery in London, *Atmospheric Environment*, 2020, **223**, 117301.
51. M. Winther, C. Dore, U. Lambrecht, J. Norris, Z. Samaras and K.-H. Zierock, EMEP/EEA air pollutant emission inventory guidebook 2023.*Journal*, 2023, DOI: https://www.eea.europa.eu/en.
52. GLA, Non-Road Mobile Machinery (NRMM) Practical Guide v.6.*Journal*, 2024, DOI: https://www.london.gov.uk/sites/default/files/2024-05/NRMM-Practical-Guide-Accessible-May2024.pdf.
53. GLA, Development sites map | London City Hall, https://www.london.gov.uk/programmes-strategies/housing-and-land/land-and-development/development-sites-map).
54. C. D. Desouza, D. J. Marsh, S. D. Beevers, N. Molden and D. C. Green, A spatial and fleet disaggregated approach to calculating the NOX emissions inventory for non-road mobile machinery in London, *Atmospheric Environment: X*, 2021, **12**, 100125.
55. UK Government, Industrial Decarbonisation Strategy.*Journal*, 2021.

56. Y. Wu, S. Zhang, J. Hao, H. Liu, X. Wu, J. Hu, M. P. Walsh, T. J. Wallington, K. M. Zhang and S. Stevanovic, On-road vehicle emissions and their control in China: A review and outlook, *Science of The Total Environment*, 2017, **574**, 332-349.

57. S. Chowdhury, S. Dey, S. N. Tripathi, G. Beig, A. K. Mishra and S. Sharma, "Traffic intervention" policy fails to mitigate air pollution in megacity Delhi, *Environmental Science & Policy*, 2017, **74**, 8-13.

58. G. Nicolini, G. Antoniella, F. Carotenuto, A. Christen, P. Ciais, C. Feigenwinter, B. Gioli, S. Stagakis, E. Velasco, R. Vogt, H. C. Ward, J. Barlow, N. Chrysoulakis, P. Duce, M. Graus, C. Helfter, B. Heusinkveld, L. Järvi, T. Karl, S. Marras, V. Masson, B. Matthews, F. Meier, E. Nemitz, S. Sabbatini, D. Scherer, H. Schume, C. Sirca, G.-J. Steeneveld, C. Vagnoli, Y. Wang, A. Zaldei, B. Zheng and D. Papale, Direct observations of CO2 emission reductions due to COVID-19 lockdown across European urban districts, *Science of The Total Environment*, 2022, **830**, 154662.

59. Y. Wu, R. Zhang, P. Tian, J. Tao, S. C. Hsu, P. Yan, Q. Wang, J. Cao, X. Zhang and X. Xia, Effect of ambient humidity on the light absorption amplification of black carbon in Beijing during January 2013, *Atmospheric Environment*, 2016, **124**, 217-223.

60. V. Ramanathan, C. Chung, D. Kim, T. Bettge, L. Buja, J. T. Kiehl, W. M. Washington, Q. Fu, D. R. Sikka and M. Wild, Atmospheric brown clouds: Impacts on South Asian climate and hydrological cycle, *Proceedings of the National Academy of Sciences*, 2005, **102**, 5326-5333.

61. W. S. Drysdale, PhD thesis, University of York, 2020.

62. B. S. Nelson, D. J. Bryant, M. S. Alam, R. Sommariva, W. J. Bloss, M. J. Newland, W. S. Drysdale, A. R. Vaughan, W. J. F. Acton, C. N. Hewitt, L. R. Crilley, S. J. Swift, P. M. Edwards, A. C. Lewis, B. Langford, E. Nemitz, Shivani, R. Gadi, B. R. Gurjar, D. E. Heard, L. K. Whalley, Ü. A. Şahin, D. C. S. Beddows, J. R. Hopkins, J. D. Lee, A. R. Rickard and J. F. Hamilton, Extreme Concentrations of Nitric Oxide Control Daytime Oxidation and Quench Nocturnal Oxidation Chemistry in Delhi during Highly Polluted Episodes, *Environmental Science & Technology Letters*, 2023, **10**, 520-527.

View Article Online
DOI: 10.1039/D5EA00039D

Data availability statements

The EddyPro software to generate fluxes and 1-D footprint can be freely download at https://www.licor.com/support/EddyPro/software.html.

The R package Openair used to generate polar plots and spatial flux footprint on map can be freely accessed at https://github.com/openair-project/openair.

NAEI data for Figure 7 has been taken from National Atmospheric Emission Inventory website: https://naei.energysecurity.gov.uk/

The ERA5 boundary layer height data can be accessed at http://cds.climate.copernicus.eu/cdsapp#!/home

The construction operation data used in this study were provided by GLA from freedom of information at (https://www.london.gov.uk/programmes-and-strategies/environment-and-climate-change/pollution-and-air-quality/nrmm).

The processed BC fluxes data are available on Centre for Environmental Data Analysis Archive (https://catalogue.ceda.ac.uk/uuid/ab605b618884401c91afd0274c92144e/).